Femtosecond spatial pulse shaping at the focal plane

Ó. Martínez-Matos,[1] P. Vaveliuk,[2*] J. G. Izquierdo,[3] and V. Loriot[4]

[1]*Departamento de Óptica, Facultad de Ciencias Físicas, Universidad Complutense de Madrid, 28040, Madrid, Spain*

[2]*Faculdade de Tecnologia, SENAI-Cimatec, Av. Orlando Gomes 1845, 41650010 Salvador, BA, Brazil*

[3] *Departamento de Química Física I, Facultad de Ciencias Químicas,Universidad Complutense de Madrid, 28040, Madrid, Spain*

[4] *Institut Lumière Matière, UMR5306 Université Lyon 1-CNRS, Université de Lyon 69622 Villeurbanne cedex, France*

[*] *pvaveliu@fis.ucm.es*

Abstract: Spatial shaping of ultrashort laser beams at the focal plane is theoretically analyzed. The description of the pulse is performed by its expansion in terms of Laguerre-Gaussian orthonormal modes. This procedure gives both a comprehensive interpretation of the propagation dynamics and the required signal to encode onto a spatial light modulator for spatial shaping, without using iterative algorithms. As an example, pulses with top-hat and annular spatial profiles are designed and their dynamics analyzed. The interference of top-hat pulses is also investigated finding potential applications in high precision pump-probe experiments (without using delay lines) and for the creation of subwavelength ablation patterns. In addition, a novel class of ultrashort pulses possessing non-stationary orbital angular momentum is also proposed. These exotic pulses provide additional degrees of freedom that open up new perspectives in fields such as laser-matter interaction and micro-machining.

OCIS codes: (050.0050) Diffraction and gratings; (070.6120) Spatial light modulators; (070.7145) Ultrafast processing; (090.1995) Digital holography; (320.5540) Pulse shaping.

References

1. D. E. Leaird and A. M. Weiner, "Femtosecond direct space-to-time pulse shaping," IEEE J. Quantum Electron. **37**, 494–504 (2001).
2. V. Loriot, O. Mendoza-Yero, G. Mínguez-Vega, L. Bañares, and R. de Nalda, "Experimental demonstration of the quasy-direct space-to-time pulse shaping principle," IEEE Photon. Technol. Lett. **24**, 273–275 (2012).
3. N. Sanner, N. Huot, E. Audouard, C. Larat, and J. -P. Huignard, "Direct ultrafast laser micro-structuring of materials using programmable beam shaping, " Opt. Laser Eng. **45**, 737–741 (2007).
4. N. Sanner, N. Huot, E. Audouard, C. Larat, J.-P. Huignard, and B. Loiseaux, "Programmable focal spot shaping of amplified femtosecond laser pulses," Opt. Lett. **30**, 1479–1482 (2005).
5. R. W. Gerchberg and W. O. Saxton, "A practical algorithm for the determination of phase from image and diffraction plane pictures," Optik **35**, 237–246 (1972).
6. S. Akturk, X. Gu, P. Bowlan, and R. Trebino, "Spacio-temporal couplings in ultrashort laser pulses," J. Opt. **12**, 093001 (2010).
7. V. Arrizón, U. Ruiz, R. Carrada, and L. A. González, "Pixelated phase computer holograms for the accurate encoding of scalar complex fields," J. Opt. Soc. Am. A **24**, 3500–3507 (2007).
8. J. A. Rodrigo, T. Alieva, A. Cámara, Ó. Martínez-Matos, P. Cheben, and M. L. Calvo, "Characterization of holographically generated beams via phase retrieval based on Wigner distribution projections," Opt. Express **19**, 6064–6077 (2011).

#194284 - $15.00 USD Received 22 Jul 2013; revised 25 Sep 2013; accepted 25 Sep 2013; published 11 Oct 2013

9. R. Borghi, F. Gori, and M. Santarsiero, "Optimization of Laguerre-Gauss truncated series," Opt. Commun. **125**, 197–203 (1996).
10. Y.-D. Liu and C. Gao, "Study on the time-varying and propagating characteristics of ultrashort pulse Laguerre-Gaussian beam," Opt. Express **18**, 12104–12110 (2010).
11. R. J. Mahon and J. A. Murphy, "Diffraction of an optical pulse as an expansion in ultrashort orthogonal Gaussian beam modes," J. Op. Soc. Am. A **30**, 215–226 (2013).
12. Y. Toda, K. Nagaoka, K. Shimatake, and R. Morita, "Generation and spatiotemporal evolution of optical vortices in femtosecond laser pulses," Electr. Eng. JPN **167**, 39–46 (2009).
13. K. Bezuhanov, A. Dreischuh, G. G. Paulus, M. G. Schätzel, and H. Walther, "Vortices in femtosecond laser fields," Opt. Lett. **29**, 1942–1944 (2004).
14. I. G. Mariyenko, J. Strohaber, and C. J. G. J. Uiterwaal, "Creation of optical vortices in femtosecond pulses," Opt. Express **19**, 7599–7608 (2005).
15. K. Bezuhanov, A. Dreischuh, G. G. Paulus, M. G. Schätzel, H. Walther, D. Neshev, W. Królikowski, and Y. Kivshar, "Spatial phase dislocations in femtosecond laser pulses," J. Opt. Soc. Am. B **23**, 26–35 (2006).
16. Ó. Martínez-Matos, J. A. Rodrigo, M. P. Hernández-Garay, J. G. Izquierdo, R. Weigand, M. L. Calvo, P. Cheben, P. Vaveliuk, and L. Bañares, "Generation of femtosecond paraxial beams with arbitrary spatial distributions," Opt. Lett. **35**, 652–654 (2010).
17. J. Atencia, M.-V. Collados, M. Quintanilla, J. Marín-Sáez, and I. J. Sola, "Holographic optical element to generate achromatic vortices," Opt. Express **21**, 21057–21062 (2013).
18. J. Strohaber, T. D. Scarborough, and C. J. G. J. Uiterwaal, "Ultrashort intense-field optical vortices produced with laser-etched mirrors," Appl. Opt. **46**, 8583–8590 (2007).
19. A. Schwarz and W. Rudolph, "Dispersion-compensating beam shaper for femtosecond optical vortex beams," Opt. Lett. **33**, 2970–2972 (2008).
20. J. Strohaber, C. Petersen, and C. J. G. J. Uiterwaal, "Efficient angular dispersion compensation in holographic generation of intense ultrashort paraxial beam modes," Opt. Lett. **32**, 2387-2389 (2007).
21. K. Bezuhanov, A. Dreischuh, G. G. Paulus, M. G. Schätzel, H. Walther, D. Neshev, W. Królikowski, and Y. Kivshar, "Spatial phase dislocations in femtosecond laser pulses," J. Opt. Soc. Am. B **23**, 26–35 (2006).
22. I. Marienko, V. Denisenko, V. Slusar, and M. Soskin, "Dynamic space shaping of intense ultrashort laser light with blazed-type gratings," Opt. Express **18**, 25143–25150 (2010).
23. J. W. Goodman, *Introduction to Fourier Optics* (McGraw Hill, 1996).
24. V. Lakshminarayanan, M. L. Calvo, and T. Alieva, *Mathematical Optics: Classical, Quantum and Computational Methods* (CRC Press, 2012).
25. E. Abramochkin, E. Razueva, and V. Volostnikov, "General astigmatic transform of Hermite-Laguerre-Gaussian beams," J. Opt. Soc. Am. A **27**, 2506–2513 (2010).
26. R. L. Phillips and L. C. Andrews, "Spot size and divergence of Laguerre Gaussian beams of any order," Appl. Opt. **22**, 643–644 (1983).
27. M. F. Erden and H. M. Ozaktas, "Accumulated Gouy phase shift in Gaussian beam propagation through first-order optical systems," J. Opt. Soc. Am. A **14**, 2190–2194 (1997).
28. A. Jefferey and H. H. Day, *Handbook of Mathematical Formulas and Integrals* (Academic Press, 2008).
29. E. Constant, A. Dubrouil, O. Hort, S. Petit, D. Descamps, and E. Mével, "Spatial shaping of intense femtosecond beams for the generation of high-energy attosecond pulses," J. Phys. B: At. Mol. Opt. Phys. **45**, 074018 (2012).
30. E. Cagniot, M. Fromager, and K. Ait-Ameur, "Modeling the propagation of apertured high-order Laguerre-Gaussian beams by a user-friendly version of the mode expansion method," J. Opt. Soc. Am. A **27**, 484–491 (2010).
31. J. T. Foley and E. Wolf, "Anomalous behavior of spectra near phase singularities," J. Op. Soc. of Am. A **19**, 2510–2516 (2002).
32. H. J. Wörner, J. B. Bertrand, D. V. Kartashov, P. B. Corkum, and D. M. Villeneuve, "Following a chemical reaction using high-harmonic interferometry," Nature **466**, 604–607 (2010).
33. R. W. Ziolkowski and J. B. Judkins, "Propagation characteristics of ultrawide-bandwidth pulsed Gaussian beams," J. Opt. Soc. Am. A **9**, 2021–2030 (1992).
34. S. Feng and H. G. Winful, "Higher-order transverse modes of isodiffracting pulses," Phys. Rev. E **63**, 046602 (2001).
35. J. C. Shane, M. Mazilu, W. M. Lee, and K. Dholakia, "Effect of pulse temporal shape on optical trapping and impulse transfer using ultrashort pulsed laser," Opt. Express **18**, 7554–7568, (2010).
36. M. Duocastella and C. B. Arnold, "Bessel and annular beams for materials processing," Laser Photonics Rev. **6**, 607–621 (2012).
37. C. Hnatovsky, V. G. Shvedov, W. Krolikowski, and A. V. Rode, "Materials processing with tightly focused femtosecond vortex laser pulse," Opt. Lett. **35**, 3417–3419 (2010).
38. J. Hamazaki, R. Morita, K. Chujo, Y. Kobayashi, S. Tanda, and T. Omatsu, "Optical-vortex laser ablation," Opt. Express **18**, 2144–2151 (2010).
39. K. Toyoda, F. Takahashi, S. Takizawa, Y. Tokizane, K. Miyamoto, R. Morita, and T. Omatsu, "Transfer of light helicity to nanostructures," Phys. Rev. Lett. **110**, 143603 (2013).

#194284 - $15.00 USD Received 22 Jul 2013; revised 25 Sep 2013; accepted 25 Sep 2013; published 11 Oct 2013

40. L. T. Vuong, T. D. Grow, A. Ishaaya, A. L. Gaeta, G. W.' t Hooft, E. R. Eliel, and G. Fibich, "Collapse of optical vortices," Phys. Rev. Lett. **96**, 133901 (2006).
41. I. J. Sola, V. Collados, L. Plaja, C. Méndez, J. San Román, C. Ruiz, I. Arias, A. Villamarín, J. Atencia, M. Quintanilla, and L. Roso, "High power vortex generation with volume phase holograms and non-linear experiments in gases," Appl. Phys. B **91**, 115–118 (2008).
42. A. Vincote and L. Bergé, "Femtosecond optical vortices in air," Phys. Rev. Lett. **95**, 193901 (2005).
43. P. Hansinger, A. Dreischuh, and G. G. Paulus, "Vortices in ultrashort laser pulses," Appl. Phys. B **104**, 561–567 (2011).
44. M. K. Bhuyan, F. Courvoisier, P.-A. Lacourt, M. Jacquot, L. Furfaro, M. J. Withford, and J. M. Dudley, "High aspect ratio taper-free microchannel fabrication using femtosecond Bessel beams," Opt. Express **18**, 566–574 (2010).
45. A. Picón, J. Mompart, J. R. Vázquez de Aldana, L. Plaja, G. F. Calvo and, L. Roso, "Photoionization with orbital angular momentum beams," Opt. Express **18**, 3660–3671 (2010).
46. C. T. Schmiegelow and F. Schmidt-Kaler, "Light with orbital angular momentum interacting with trapped ions," Eur. Phys. J. D **66**, 157 (2012).

1. Introduction

Nowadays, phase-only 2D spatial light modulators (SLMs) have become an essential tool for modulation and analysis of light. The SLMs are applied in many areas of optics highlighting beam optics, optical tweezers and adaptive optics. Most applications are devoted to monochromatic light, but in the last decades, SLMs applied to temporal pulse shaping, such as the direct space-to-time [1] and quasy-direct space-to-time pulse shapers (see [2] and references therein), has become a reality. But less effort has been devoted to spatial pulse shaping. In spite of this, pulse shaping in the spatial domain preserving the temporal behavior of the incoming pulses has become a feasible tool for femtosecond laser micro-machining [3, 4]. The efforts have been focused on determining the signal to be applied to the SLM for obtaining the desired intensity distribution at the focal plane [4]. Appropriate algorithms to solve the phase retrieval problem developed for monochromatic light, such as the Gerchberg-Saxton [5], have been used satisfactory for pulses >130 fs. But these algorithms fail for shorter pulses due to the spatio-temporal coupling [6] and they are limited to intensity calculation at the focus, losing the phase information of the wavefields.

In this paper, a procedure is theoretically analyzed to overcome these limitations by 1) encoding a complex signal, amplitude and phase, onto phase-only computer generated holograms by the method proposed in [7,8], and 2) expanding the signal in an orthonormal basis composed of Laguerre-Gaussian (LG) modes. This procedure gives a direct interpretation of the propagation dynamics of ultrashort laser pulses at the focus. In adition, it allows directly finding the signal to be encoded onto the SLM for pulse shaping in the spatial domain without using hard iterative algorithms. These advances are useful in a large variety of engineering and industrial applications as well as in fundamental physical and chemical ultrafast phenomena.

The expansion of light fields in LG modes is a well known technique used mostly for monochromatic light [9], with the exception of a few works in which this is employed to analyze the dynamics of ultrashort pulses [10, 11]. In [10], Liu *et al* determine the propagation of the ultrashort pulse Laguerre-Gaussian Beam. The authors consider non-constant expansion coefficients dependent on space-time variables, whose solutions are found numerically. In [11], Mahon et al use the expansion method to find the diffraction of ultrashort pulses by amplitude modulating transmittances. The procedure in [11] is quite different to that in [10] since the expansion coefficients are taking as constant values, while the expansion elements (the orthonormal basis) are space-time dependent. Their results were not computational efficient, as pointed out by the authors, for the reason that the expansion elements were calculated numerically. We extend the procedure described in [11] to determine the diffraction of pulses by complex signals codified in computer generated holograms. Each element of the expansion at the SLM

#194284 - $15.00 USD Received 22 Jul 2013; revised 25 Sep 2013; accepted 25 Sep 2013; published 11 Oct 2013

plane is propagated to the focus being univocally associated to its corresponding ultrashort electric field, the "pulselet". The pulse is then the finite sum of the individual pulselets weighted by the expansion coefficients. This simples result directly relates the signal at the SLM with the diffracted ultrashort wavefields. We obtain closed-form expressions for the pulselets, and therefore, the expansion method becomes extremely efficient and physically intuitive.

This procedure is not limited to direct pulse propagation. It can also be applied to solve the inverse problem, which to our knowledge is an original finding. That is, the proper signal for spatial shaping at the focus is found directly without using iterative algorithms (developed for monochromatic light) to solve the phase retrieval problem. Consequently, the applicability of the method includes very short pulses with broad spectral bandwidth. Besides, this method calculates the electric field, opening the window to control the spatial phase of the pulses just by using SLMs. This fact permits to design complex ultrashort wavefield structures in a very simple manner, such as the ones suggested in Section 5.

This work is organized as follows. Section 2 reviews the optical setups in which the SLM can be implemented to avoid angular dispersion and spatial chirp. In Section 3, the connection between the signal at the SLM and the pulse at the focus is derived. A closed-form expression for the pulselets is then given and its main features, such us the space-time coupling and the orbital angular momentum (OAM), are analyzed in Section 4. In Section 5 some representative examples of ultrashort spatial pulse shaping are shown. The generation of spatial top-hat ultrafast beam profiles and the interference of this class of pulses are included as examples, showing its potential applications to high precision pump-probe experiments without using delay lines and also to the creation of subwavelength ablation patterns in an approach with no moving parts. In this section the creation of spatial annular ultrafast beam profiles is also included, showing the versatility of the procedure. In addition, a novel class of ultrashort pulses possessing non-stationary OAM with unique properties is also proposed. Finally, discussion and concluding remarks are given in Section 6.

2. Optical setup

In phase-only computer generated holograms, the signal is encoded onto the 2D SLM with a carrier frequency (a grating working in the first order of diffraction) to isolate the desired field from the other diffraction orders. These holograms work properly for monochromatic light. But, in ultrashort pulse applications, with broad spectral bandwidth, this encoding method makes the hologram dispersive as pointed out in [12]. It is necessary to introduce an extra optical element, as a grating with a carrier frequency equal to the one on the SLM, to create an identical angular dispersion with reverse sign to cancel out the whole angular dispersion at the output plane of the SLM. This configuration is schematically represented in Fig. 1(a), where the grating G and the SLM are respectively located at the input and output planes of an imaging optical system. The angular dispersion on G is then reverted and the system images the input field at the grating in the SLM, avoiding spatial chirp due to light propagation between the planes. The imaging optical systems proposed in the literature are a 4f setup [13], a 2f-2f setup [14] and a double pass grating compressor, which is not exactly an imaging system [15]. Other configurations such as a lens-less setup with grating and SLM assembled [16, 17] and modifications based on the scheme in Fig. 1(a) have been also reported [18–22]. In Fig. 1(a), it has been considered that the pulse diffracted by the SLM is Fourier Transform Limited (FTL). This condition can be reached by applying appropriately chirps to the incoming laser pulses to compensate the temporal modification due to light propagation between G and the SLM. Any of these approaches spatially shape the spectral components of the pulse at the SLM without angular dispersion and without spatial chirp. These conditions are mandatory for a proper spatial pulse shaping at the focal plane.

#194284 - $15.00 USD Received 22 Jul 2013; revised 25 Sep 2013; accepted 25 Sep 2013; published 11 Oct 2013

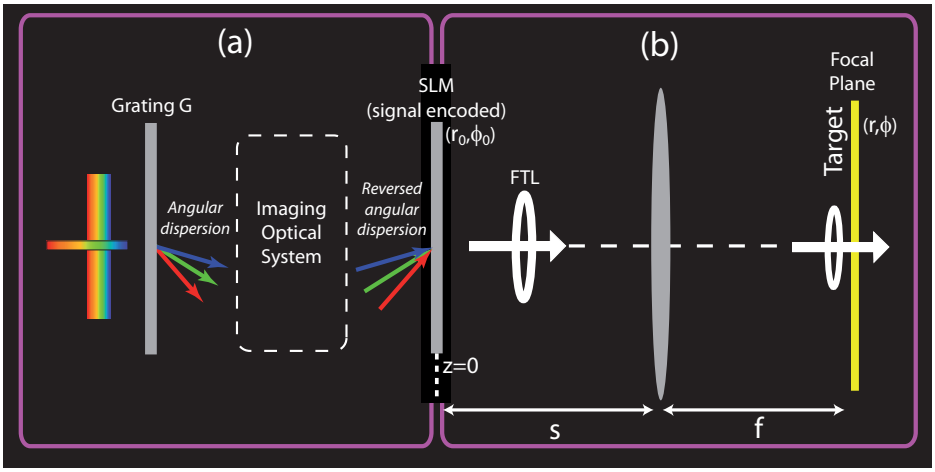

Fig. 1. (a) Approach to implement the encoded signal in phase-only computer generated holograms to the whole spectrum of the pulse. The imaging optical system cancels out the spatial chirp at the 2D SLM and makes the approach nondispersive. (b) Typical arrangement for laser micro-machining in which the spatial pulse shaping at the focus is desired.

Our proposal is experimentally realizable with current technology. Phase gratings (constant signal) encoded onto phase only 2D SLMs can diffract light with efficiencies reaching 40% or even more. But these values can be dropped when the spatial structure of the signal is hard, involving for example secondary maximum and minimum with amplitudes much smaller than the central lobe. It occurs when spatial top-hat or annular ultrafast beam profiles are created at the focal plane of a convergent lens, as it will be discussed in Section 5. This drawback can be removed by just matching the spatial half-width at half-maximum (HWHM) of the input pulse with the central lobe HWHM of the signal reducing drastically the diffraction losses. This can be easily done by selecting the proper focal lens to adapt the required signal to the input pulse dimension, whose HWHM is often higher than 2 mm. This condition assures that the signal is correctly sampled by the discretization of the SLM chip. On the other hand, most commercial SLMs operate dephasing the light up to a range of 2π radians distributed in 256 (8-bit) gray levels, allowing a proper sampling for the secondary maximum analyzed in the examples of this work. Spatial shaping of ultrashort pulses at the focus of a convergent lens using SLMs is feasible to be realized experimentally with current state-of-the-art technology.

3. Relationship between signal and pulse via the LG modes

Using any of the approaches described in Section 2, the diffracted field, E_0, corresponding to each frequency component ω at the SLM plane ($z=0$), can be written in cylindrical coordinates (r_0,ϕ_0) as

$$E_0(\omega,r_0,\phi_0,z=0)=S(\omega)\exp\left(-\frac{r_0^2}{\beta^2}\right)R'(r_0,\phi_0), \tag{1}$$

where $S(\omega)$ is the spectral amplitude of the input pulse and $R'(r_0,\phi_0)$ is the encoded complex signal in the dynamically controllable hologram. It has been considered an incident pulse with Gaussian spatial distribution whose beam waist size, β, is identical for all spectral components being the waist located at the SLM plane. Under these assumptions we define $R'(r_0,\phi_0)=\exp\left(r_0^2/\beta^2\right)R(r_0,\phi_0)$, to compensate the spatial distribution of the incident pulse and get the field,

#194284 - $15.00 USD Received 22 Jul 2013; revised 25 Sep 2013; accepted 25 Sep 2013; published 11 Oct 2013

$$E_0(\omega, r_0, \phi_0, z=0) = S(\omega) R(r_0, \phi_0), \tag{2}$$

which is proportional to the desired signal, $R(r_0, \phi_0)$, for the whole spectrum. A proper choice of $R(r_0, \phi_0)$ modulates spatially the pulse at the focal plane achieving the required spatial distribution.

Figure 1(b) shows the typical arrangement for femtosecond laser machining. The convergent lens of focal length f is placed at the distance s from the SLM being the field evaluated at the focal plane $z = s + f$. The field propagation is described by the paraxial theory considering nondispersive aberration-less lenses, such as dichroic lenses or spherical mirrors. Under such conditions, the field at the focus expressed in cylindrical coordinates (r, ϕ), is

$$E(r, \phi, s+f; \omega) = P(r; \omega) FT\left[E_0(r_0, \phi_0, z=0; \omega)\right], \tag{3}$$

where

$$P(r; \omega) = -i\frac{\omega}{2\pi c f} \exp\left[i\frac{\omega}{c}(s+f)\right] \exp\left[i\frac{\omega}{2fc}\left(1 - \frac{s}{f}\right) r^2\right] \tag{4}$$

is defined by the arrangement geometry [23] and FT is the spatial Fourier Transform operator that relates the field at the SLM with the field at the focal plane.

The total scalar electric field at the focus, $\mathscr{E}$, as a function of the temporal and spatial coordinates is obtained by integrating (3) on the whole frequency range as

$$\mathscr{E}(t, r, \phi, s+f) = \frac{1}{2\pi} \int_{-\infty}^{\infty} E(r, \phi, s+f; \omega) \exp(-i\omega t)\, d\omega. \tag{5}$$

Numerical integration of (5) is a cumbersome problem. An alternative method to find the diffraction of optical pulses by hard apertures were proposed recently in [11], in which the diffracted ultrashort pulses are obtained propagating the basis elements of the aperture expansion in terms of LG modes. This procedure were not computational efficient since the analytical expression for the propagation of the LG ultrashort pulses, the pulselets, were undiscovered. The key is to find the analytical expression of the pulselets to connect, in a intuitive for a physical viewpoint and numerically efficient method, the signal at the SLM and the pulsed field at the focus via the expansion coefficients in terms of LG modes.

Thus, the signal at the SLM is written as

$$R(r_0, \phi_0) = \sum_{n,m=0}^{\infty} A_{n,m} LG_{n,m}(r_0, \phi_0; w_0), \tag{6}$$

with $LG_{n,m}$ being the Laguerre-Gaussian beams of an orthonormal base explicitly giving by [24]

$$LG_{n,m}(r_0, \phi_0; w_0) = \sqrt{\frac{2^{|m|+1} n!}{\pi (n+|m|)!}} \frac{\exp(im\phi_0)}{w_0^{|m|+1}} r_0^{|m|} L_n^{(|m|)}\left(\frac{2r_0^2}{w_0^2}\right) \exp\left(-\frac{r_0^2}{w_0^2}\right). \tag{7}$$

The wavefield at the focus can be written as

$$\mathscr{E}(t, r, \phi, s+f) = \sum_{n,m=0}^{\infty} A_{n,m} \mathscr{LG}_{n,m}(t, r, \phi, s+f), \tag{8}$$

being easily interpreted as the weighted sum of the propagated LG pulselets,

$$\mathscr{LG}_{n,m}(t, r, \phi, s+f) = \frac{1}{2\pi} \int_{-\infty}^{\infty} S(\omega) P(r; \omega)\, TF\left[LG_{n,m}(r_0, \phi_0; w_0)\right] \exp(-i\omega t)\, d\omega. \tag{9}$$

#194284 - $15.00 USD Received 22 Jul 2013; revised 25 Sep 2013; accepted 25 Sep 2013; published 11 Oct 2013

Notice that the signal and the pulse are simply linked by the expansion coefficients $A_{n,m}$ whose explicit expression is

$$A_{n,m} = \int_0^{2\pi} \left(\int_0^{\infty} R(r_0, \phi_0)\, LG^*_{n,m}(r_0, \phi_0; w_0)\, r_0 dr_0 \right) d\phi_0. \tag{10}$$

The $LG_{n,m}$ modes of the expansion, with radial n, and azimuthal m indexes have a doughnut-shaped beam profile with a OAM of order m (topological charge m). In (7), w_0 is the beam waist size of the expansion elements and $L_n^{(|m|)}$ is the modified Laguerre polynomial.

Taking into account the spatial Fourier Transform of the LG modes [25],

$$TF\left[LG_{n,m}(r_0, \phi_0; w_0)\right] = (-i)^{2n+|m|} \frac{2\pi c f}{\omega} LG_{n,m}(r, \phi; w), \tag{11}$$

where the new beam waist is $w = 2fc/w_0\omega$, one can finally obtain the expression for the pulselets:

$$\mathscr{LG}_{n,m}(t, r, \phi, s+f) = (-i)^{2n+|m|}\, cf \int_{-\infty}^{\infty} \frac{S(\omega)}{\omega} P(r;\omega)\, LG_{n,m}(r, \phi; w) \exp(-i\omega t)\, d\omega. \tag{12}$$

In summary, the propagation of the pulse to the focus is just found by calculating the coefficients $A_{n,m}$ that relate the signal at the SLM (6) to the wavefield at the focus (8). It could be said that the spatio-temporal features of the pulse are fully described by the pulselets $\mathscr{LG}_{n,m}$, allowing a physically intuitive representation of the field.

4. Pulselets features

In this section, the analytical expressions for the pulselets are derived. For comparative purposes, it is analyzed first the singular case of the monochromatic beam with spectrum $S(\omega) = \delta(\omega - \omega_0)$. According to (12) the wavelet (the monochromatic pulselet) $\mathscr{LG}^{Mon}_{n,m}$, can be written as

$$\mathscr{LG}^{Mon}_{n,m}(t, r, \phi, s+f) = (-i)^{2n+|m|+1} (2\pi)^{-1} \exp(-i\omega_0 t_p)\, LG_{n,m}(r, \phi; w_1), \tag{13}$$

where $w_1 = 2fc/w_0\omega_0$ is the beam waist size at the focal plane for the angular frequency ω_0, and

$$t_p = t - \frac{s+f}{c} - \frac{1}{2fc}\left(1 - \frac{s}{f}\right) r^2 \tag{14}$$

is a position-dependent delay time. $\mathscr{LG}^{Mon}_{n,m}$ is a LG beam with transverse extension characterized by the effective radius [26], $\beta_m = w_1\sqrt{2|m|+1}$, and it is affected by a spherical phase, $(\omega_0/2fc)(1 - s/f) r^2$ giving by (14) that slightly shifts the beam focus towards higher distances. In this case the focal plane, $z = s + f$, and the beam focus are not coincident. The factor $(-i)^{2n+|m|+1}$ in (13) appears to be the accumulated Gouy phase shift [27] in the propagation of each LG beam from its waist (at the SLM) to the focal plane.

Let us now find the pulselets $\mathscr{LG}_{n,m}$. We describe the propagation by a conventional temporal Gaussian signal:

$$s(t) = \exp\left(-\frac{t^2}{\tau_0^2}\right) \exp(-i\omega_0 t), \tag{15}$$

where $\sqrt{\ln 2}\,\tau_0$ is the HWHM of the Gaussian signal and ω_0 is the central angular frequency. The analytical expression for the pulselets is deduced expanding the modified Laguerre polynomial

#194284 - $15.00 USD Received 22 Jul 2013; revised 25 Sep 2013; accepted 25 Sep 2013; published 11 Oct 2013

in a power series in (12), performing the integral and taking into account the Rodrigues formula [28], giving

$$\mathscr{LG}_{n,m}(t,r,\phi,s+f) = (-1)^{n+|m|+1}\sqrt{\frac{n!}{2\pi(n+|m|)!}}\frac{1}{\rho_0}\left(\frac{\tau_0}{\tau_1}\right)^2$$

$$\times\exp\left[-\left(\frac{\tau_0}{\tau_1}\right)^2\frac{r^2}{w_1^2}\right]\exp(im\phi)\exp(-i\omega_1 t_p)\exp\left(-\frac{t_p^2}{\tau_1^2}\right)$$

$$\times\sum_{p=0}^{n}\left(\begin{array}{c} n+|m| \\ p+|m| \end{array}\right)\frac{1}{p!}\left[\left(\frac{\tau_0}{\tau_1}\right)^2\frac{r}{\sqrt{2}\rho_0}\right]^{2p+|m|}H_{2p+|m|+1}\left(\frac{t_p+i\frac{\omega_0}{2}\tau_0^2}{\tau_1}\right), \tag{16}$$

where

$$\tau_1 = \tau_0\sqrt{1+\left(\frac{r}{\rho_0}\right)^2}, \tag{17}$$

is a position-dependent time constant, $\omega_1 = \omega_0\tau_0^2/\tau_1^2$ is a position-dependent angular frequency, $H_l(.)$ is the Hermite polynomials of index l and $\rho_0 = fc\tau_0/w_0$ is a constant that normalizes the transverse distance r/ρ_0. Equation (16) reduces to (13) when $\tau_0 \to \infty$.

Equation (16) is a key result since it states the pulselets by means of an analytical expression. The pulselets are space-time localized wave packets propagating in free space. Their spatio-temporal features are mainly driving by the term t_p/τ_1 in (16). The exponential factor $\exp\left(-t_p^2/\tau_1^2\right)$ delays the wave packets by a constant time $(s+f)/c$, which is removed for simplicity, and by the spherical arrival-time $(1/2fc)(1-s/f)r^2$. In the case $s=f$, the pulse peak follows on a plane arrival time. The spatial distribution of the pulselets are formed by the finite combination of the Hermite polynomials $H_l(t_p/\tau_1)$. In addition, the OAM of the pulselets is defined by $\exp(im\phi)$. As it has the same order m than the $LG_{n,m}$ mode, the OAM is preserved in the propagation of each pulselet to the focus.

To illustrate the pulselets properties described above, the monochromatic wavelet $\mathscr{LG}_{5,3}^{Mon}$ is compared with its counterpart, the pulselet $\mathscr{LG}_{5,3}$. This is a representative case because exhibits an appreciable OAM (order $m=3$) and a complex intensity profile composed by six concentric rings ($n=5$), see Fig. 2(a). The parameters used in the simulations are feasible to be experimentally realized, $f=15$ cm, $\tau_0=15$ fs, $\lambda_0=800$ nm and $w_0=150\,\mu$m. For these values it is obtained $\rho_0=4.5$ mm and a transverse extension characterized by the effective radius, $\beta_3\sim 670\,\mu$m for the $\mathscr{LG}_{5,3}^{Mon}$ mode. Notice that the time constant and the angular frequency evaluated at the distance β_3 are $\tau_1=15.16$ fs and $\omega_1=2.30\,10^{15}$ Hz, very close to $\tau_0=15.00$ fs and $\omega_0=2.36\,10^{15}$ Hz, respectively. Thus, it is expected that the pulse duration and the angular frequency at positions where the intensity is non-negligible slightly differs from the original values of the incident pulse.

In Fig. 2(b) the intensity evolution of $\mathscr{LG}_{5,3}^{Mon}$ for $s=f$ is depicted, while Figs. 2(c)-2(d) display the intensity evolution of $\mathscr{LG}_{5,3}$, computed from (16), for the cases $s=f$ and $s=5f$, respectively. These are representative cases because the way in which the pulse arrives to the focal plane varies depending on the value s, as it will be shown below. In these figures, the axial extent is displayed in relation to β_3, while the temporal axis is in terms of the time duration τ_0 of the input signal. The dashed lines delimits the temporal HWHM centered on the pulse peak intensity. As illustrated, plots along the spatial coordinate in Figs. 2(b)-2(c) are very similar when evaluated at $t=0$. This is because the rings of the pulselet arrive at the focal plane simultaneously, no matter the transverse position. The case $s=5f$ does not meet this condition

#194284 - $15.00 USD Received 22 Jul 2013; revised 25 Sep 2013; accepted 25 Sep 2013; published 11 Oct 2013

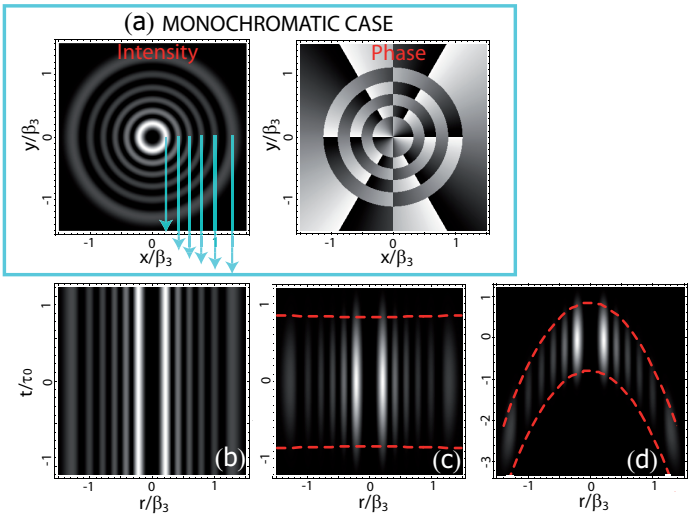

Fig. 2. (a) Instantaneous intensity and phase for the monochromatic case $\mathscr{LG}^{Mon}_{5,3}$ with $s = f$, normalized to the spatial extent in Cartesian coordinates. Intensity evolution of the wavelet $\mathscr{LG}^{Mon}_{5,3}$ (b) and the pulselet $\mathscr{LG}_{5,3}$ for the arrangements (c) $s = f$ and (d) $s = 5f$ as a function of the normalized time and spatial extent. Arrows connect the rings in Cartesian coordinates (a) with the rings in the space-time representation (b) for the monochromatic case. Dashed lines delimits the temporal HWHM centered on the pulse peak intensity. Intensity graphs are normalized to its maximum value, while the gray-scale in the phase representation runs from $-\pi$, black, to $+\pi$, white, radians. The parameters are $f = 15$ cm; $w_0 = 150\,\mu$m; $\tau_0 = 15$ fs; $\lambda_0 = 800$ nm and $\beta_3 = 670\,\mu$m.

and the pulse rings follow a spherical arrival-time [see Fig. 2(d)]. The pulse delay from $r = \beta_3$ to the center, $r = 0$, is $t_p \sim 20$ fs, higher than τ_0. Therefore, the shape of the instantaneous intensity at the focal plane changes very quickly in time as it is highlighted by the dashed line on Fig. 2(d).

A detailed analysis of the spatial distribution of intensity and phase in Cartesian coordinates is displayed in Fig. 3 by different snapshots. Figure 3(a) shows the pulselets in the arrangement $s = f$ evaluated at $t = -\tau_0, 0, \tau_0$, while in Fig. 3(b) it is displayed the case $s = 5f$ evaluated at the times $t = -2.5\tau_0, -\tau_0, 0, \tau_0$. The snapshot $t = -2.5\tau_0$ in Fig. 3(a) has been not represented because of the intensity at this time is negligible. For comparative purposes the monochromatic case with $s = f$ is also depicted. As illustrated, the intensity distribution in Fig. 3(a) for $t = 0$ is very close to the intensity of $\mathscr{LG}^{Mon}_{5,3}$, but it slightly differs for $t = -\tau_0$ and $t = \tau_0$, in accordance with Fig. 2. Besides, the phase at $t = 0$ is almost identical to the one of the monochromatic case, while in previous and latter times it acquires a spherical phase, convergent for $t = -\tau_0$ and divergent for $t = \tau_0$. The pulselet evolves first converging to the focal plane until the phase become plane, beginning to diverge in a posterior time. This is the optimal experimental configuration: the instantaneous intensity of the pulselet is as close as possible to its monochromatic counterpart. Pulselets with $s = 5f$ behave quitte different. Its peak intensity has a spherical arrival-time. Hence, the larger diameter ring appears first and, as the pulse evolves in time, the most close to the center appears at latter times. Such a behavior is interpreted as following: the pulse get into focus in a plane different to the focal plane. Thus, there is a spherical phase at all times analyzed, as the first line of Fig. 3(b) points out.

In Figs. (2)-(3), the main properties of the pulselets with a small waist size value at the SLM,

#194284 - $15.00 USD Received 22 Jul 2013; revised 25 Sep 2013; accepted 25 Sep 2013; published 11 Oct 2013

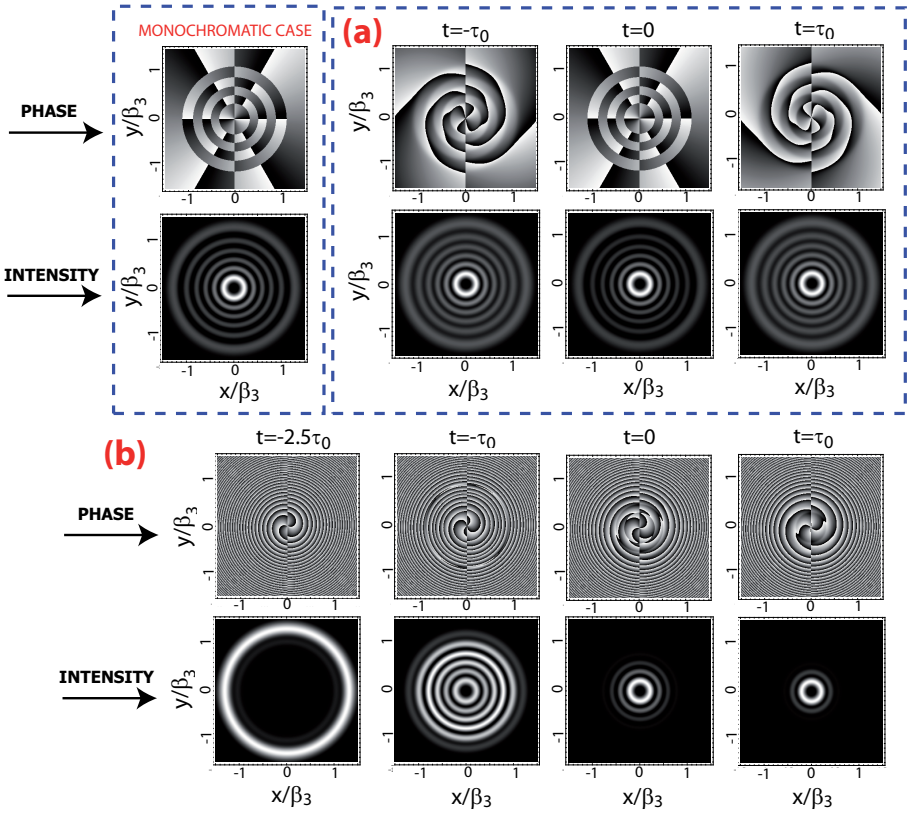

Fig. 3. Intensity and phase in Cartesian coordinates for the pulselet $\mathscr{LG}_{5,3}$ evaluated at the snapshots indicated in the figure with (a) $s = f$ and (b) $s = 5f$. It is also displayed the instantaneous intensity and phase for the monochromatic case $\mathscr{LG}_{5,3}^{Mon}$ with $s = f$. Intensity graphs are normalized to its maximum value, while the gray-scale in the phase representation runs from $-\pi$, black, to $+\pi$, white, radians. Parameters are the same than in Fig. 2.

$w_0 = 150\,\mu$m, was used. As pointed out in (6), the pulselets features characterize the space-time dependence of the wavefield at the focus through the expansion method. It is then convenient to analyze the properties of the pulselets when the waist size dimension of the LG expansion is relatively large, $w_0 = 3$ mm. In this case, a small transverse extension characterized by the effective radius, $\beta_3 \sim 34\,\mu$m, has been obtained. The spatio-temporal evolution of the pulselet is carried out by t_p/τ_1, that is independent on w_0 when evaluated at β_3. Thereby, the instantaneous intensity of $\mathscr{LG}_{5,3}$ for $s = f$ is also represented by Fig. 2(a) and Fig. 3(a), both scaled by the new value β_3. When $s = 5f$, the delayed spherical arrival-time evaluated at β_3 is $\sim 10^{-2}$ fs, which is negligible compared to τ_0. The pulse peak follows on an approximate plane arrival-time so that the pulselet features are close to the case $s = f$. This conclusion also applies to longer pulses, shorter focal distances and larger beam waist size at the SLM.

5. Spatial pulse shaping at the focus

Section 3 describes the ultrashort pulse at the focus using the signal expansion in a LG basis. But nothing was said about the proper signal to generate the required spatial field distribution at the focal plane, say $f(r,\phi)$. To this, $f(r,\phi)$ must be expanded in terms of a LG basis particularized

#194284 - $15.00 USD Received 22 Jul 2013; revised 25 Sep 2013; accepted 25 Sep 2013; published 11 Oct 2013

for the central frequency ω_0:

$$f(r,\phi) = \sum_{n,m}^{\infty} B_{n,m} LG_{n,m}(r,\phi;w_1), \tag{18}$$

finding the new expansion coefficients $B_{n,m}$. The relationship between $B_{n,m}$ and $A_{n,m}$ can be derived by comparing (18) with the wavefield at the focus for the central frequency, $\mathscr{E}_{Mon}$, evaluated in $t = 0$:

$$\mathscr{E}_{Mon}(0,r,\phi,s+f) \propto \exp\left[\frac{i\omega_0}{2fc}\left(1-\frac{s}{f}\right)r^2\right] \sum_{n,m}^{\infty} A_{n,m}(-i)^{2n+|m|+1} LG_{n,m}\left(r,\phi;\frac{2fc}{w_0\omega_0}\right), \tag{19}$$

obtaining that

$$A_{n,m} \propto (-i)^{-2n-|m|-1} B_{n,m} \exp\left[-\frac{i\omega_0}{2fc}\left(1-\frac{s}{f}\right)r^2\right], \tag{20}$$

and $w_0 = 2fc/w_1\omega_0$. The ultrashort spatial pulse at the focus is then computed by (8) and the signal to be codified in the dynamically controllable hologram is found by (6), in both cases using the coefficients $A_{n,m}$ giving by (20). This approach avoids a hard calculation arose from the iterative algorithms used to solve the inverse problem. Notice that these algorithms developed for monochromatic light, for example [5], are limited to pulses > 130 fs and they only compute the instensity distribution at the focus. By the procedure described above, these limitations are overcomed since the electric field of the ultrashort pulse for any pulse duration is obtained directly.

In the next section some representative examples of ultrashort spatial pulse shaping at the focus via complex signals are shown. The space-time dependence of the ultrashort pulse will be found for $s = f$. This condition simplifies (20) to $A_{n,m} \propto (-i)^{-2n-|m|-1} B_{n,m}$. For comparative purposes, the same coefficients $A_{n,m}$ will be used to find the pulses for $s = 5f$. The parameters in the simulations are the same than in Section 4.

5.1. Spatial top-hat and annular ultrafast beam profiles

Let us create spatial top-hat ultrafast beam profiles at the focus by the method proposed in this work. This profile was chosen because it has been wide used for material processing applications [3] and for high harmonic generation [29].

The LG expansion of the spatial top-hat profile of radius a is calculated at the focal plane considering $s = f$. This profile has no OAM so that the terms of the expansion with $m \neq 0$ are identically zero. The coefficients $B_{n,0}$ are shown in the inset of Fig. 4(a) evaluated for $a = 1.4$ mm and a finite numbers of terms giving by $M = 30$. Following [11], the beam waist size of the expansion that better fits the truncated series is $w_1 = 255\,\mu$m, corresponding to the value $w_0 = 150\,\mu$m at the SLM. The finite series is obtained by changing the ∞ in the summation operator in (6) and (8) by the finite number M. In Fig. 4(a), the ideal top-hat (thick gray line) is compared to the fitting (blue line), while Fig. 4(b) compares the signal (thick gray line) at the SLM, obtained by Fourier Transforming the top-hat function $[R(r_0,\phi_0) \propto J_1(\omega_0 ar/cf)/(\omega_0 ar/cf)]$, to the LG expansion (blue line) calculated with $w_0 = 150\,\mu$m and the coefficients $A_{n,m}$ giving by (20). Notice that the signal in Fig. 4(b) should be encoded in computer generated holograms with the carrier frequency (not shown on the figure) following the procedure [7, 8]. The normalized mean square error for the truncated series, ε_M, is [30]

$$\varepsilon_M = 1 - \frac{1}{\|U\|^2} \sum_{n,m}^{M} B_{n,m}^2, \tag{21}$$

#194284 - $15.00 USD Received 22 Jul 2013; revised 25 Sep 2013; accepted 25 Sep 2013; published 11 Oct 2013

where $\|U\|^2$ is the integration of the square modulus of the original function over the whole transverse plane. The value obtained is $\varepsilon_{30} = 0.0096$ indicating that the fitting deviates from the original function less than 1%. We obtain a good fitting by $M = 30$, a reasonable low value to the method be numerically highly efficient.

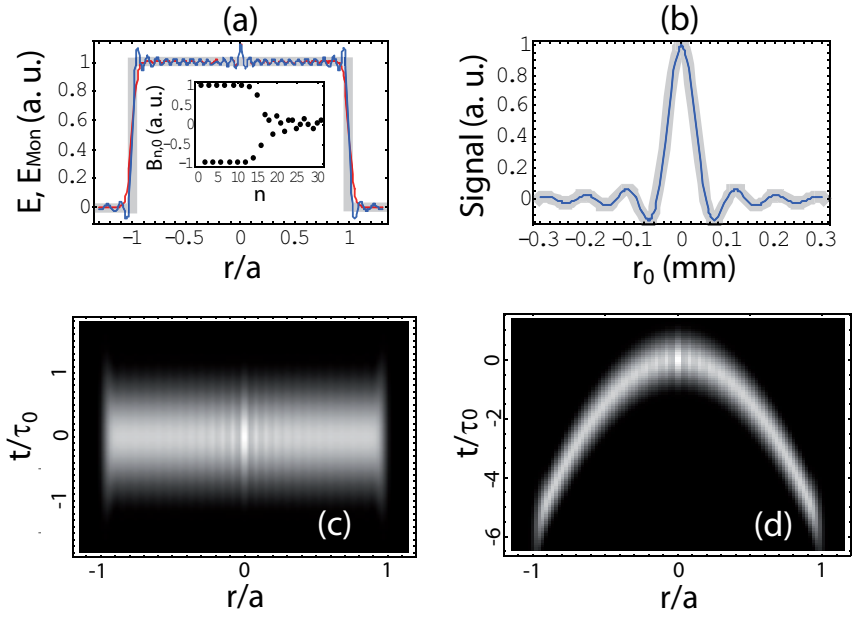

Fig. 4. (a) Top-hat beam profile (thick gray line) at the focal plane and the LG expansion (blue line) computed for 31 terms using the normalized coefficients $B_{n,0}$ shown in the inset. The field of the ultrashort pulse evaluated at $t = 0$ (red line) also shows a top-hat beam profile. (b) Signal to be encoded in the computer generated hologram obtained by Fourier Transforming the top-hat function (thick gray line) and its expansion (blue line) using the same numbers of terms. Instantaneous intensity of the pulse at the focus as computed by (8) using the coefficients of the inset for (c) $s = f$ and (d) $s = 5f$. In Fig. 4(a) and Figs. 4(c)-4(d) the axial extents are shown in relation to the radius $a = 1.4$ mm and the parameters are the same than in Fig. 2.

The field of ultrashort pulse for $t = 0$, as computed by (8), is shown by the red line in Fig. 4(a). The spatial profile is represented aproximated by a top-hat function, too. Besides, the temporal evolution of the intensity of the pulse is displayed in Fig. 4(c), showing that the profile at any time is an approximated top-hat function although the pulse duration is widened in $r \sim a$. This phenomenon is related to the spectral anomalies [31], that is, each component of the spectrum at the focal plane is centered at $r = 0$, but the spatial profile is scaled by the value of the frequency. It is enhanced in points where the field amplitude for the central frequency varies quickly in its neighborhood, $r \sim a$. This result in a local variation of the spectrum that modifies the pulse duration, as shown in Fig. 4(c). For comparative purposes the intensity of the pulse for the case $s = 5f$ is shown in Fig. 4(d) using the same coefficients $B_{n,0}$. A spherical arrival-time is followed by the pulse, but maintains the top-hat spatial profile. It has been demonstrated that spatial top-hat ultrafast beam profiles can be easily generated by 2D SLMs and computed efficiently by the LG expansion method.

It is interesting to analyze the top-hat expansion up to $M = 30$ possessing smaller radius, $a = 70\,\mu$m. In this case, the best fitting beam waist size is $w_1 = 12.7\,\mu$m, corresponding to

#194284 - $15.00 USD Received 22 Jul 2013; revised 25 Sep 2013; accepted 25 Sep 2013; published 11 Oct 2013

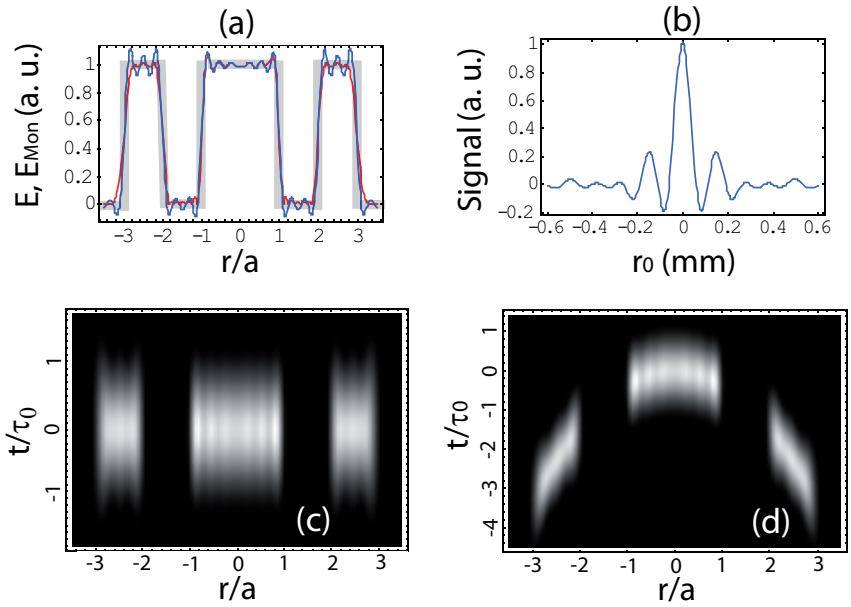

Fig. 5. (a) Top-hat and annular beam profile (thick gray line) at the focal plane and the LG expansion (blue line) computed for 31 terms. The field of the ultrashort pulse evaluated at $t = 0$ (red line) shows a similar profile. (b) Expansion of the signal to be encoded in the computer generated hologram using the same numbers of terms. Instantaneous intensity of the pulse at the focus as computed by (8) for (c) $s = f$ and (d) $s = 5f$. In Fig. 5(a) and Figs. 5(c)-5(d) the axial extents are shown in relation to the radius $a = 350\,\mu$m and the parameters are the same than in Fig. 2.

$w_0 = 3$ mm at the SLM. As discussed in Section 4, the behavior of the pulselets with $w_0 = 3$ mm for $s = f$ and $s = 5f$ are very similar. The same behavior is then expected for a top-hat ultrafast beam profile. This statement can be demonstrated by a direct substitution of the new parameters in (8). Hence, both cases, $s = f$ and $s = 5f$, are represented by Fig. 4(c) but normalized by the new value $a = 70\,\mu$m.

Let us now study a hard spatial function computed by $M = 30$. This function is composed by a top-hat with radius $a = 350\,\mu$m and a single-annular beam of width a. The best fitting beam waist size at the focal plane is the same than in Fig. 4, $w_1 = 255\,\mu$m. The results by performing an equivalent analysis to that performed in Fig. 4, are shown in Fig. 5. A good fitting ($\varepsilon_{30} = 0.033$) is obtaining by just using 31 terms, even for hard functions with sharp edges.

5.2. *Interference of spatial top-hat ultrafast beam profiles*

In above examples the signal was centered on the optical axis of the system, $r_0 = 0$. A displacement of the signal by a distance $\pm b$ from $r_0 = 0$ along a transverse axis of the SLM, says x_0, generates a $\exp(\pm i\omega bx/fc)$ phase at the focal plane, in accordance with the shift property of the Spatial Fourier Transform [23]. This phase term modifies the position-dependent delay time,

$$t_p^{\pm}(t,r) = t - \frac{s+f}{c} - \frac{1}{2fc}\left(1 - \frac{s}{f}\right)r^2 \pm \frac{b}{fc}x. \tag{22}$$

#194284 - $15.00 USD Received 22 Jul 2013; revised 25 Sep 2013; accepted 25 Sep 2013; published 11 Oct 2013

The pulse at the focal plane is computed by (8), with the coefficients $A_{n,m}$ being calculated according to Section 5.1, and the pulselets giving by (16) with $t_p \to t_p^{\pm}$. The temporal evolution of the intensity as a interference of two spatial top-hat ultrafast beams with $a = 1.4$ mm, is shown in Fig. 6(a), while Fig. 6(b) depicts the interference of two top-hats having a size of $a = 70\,\mu$m. In these plots $s = f$ and $b = \pm 1.4$ mm.

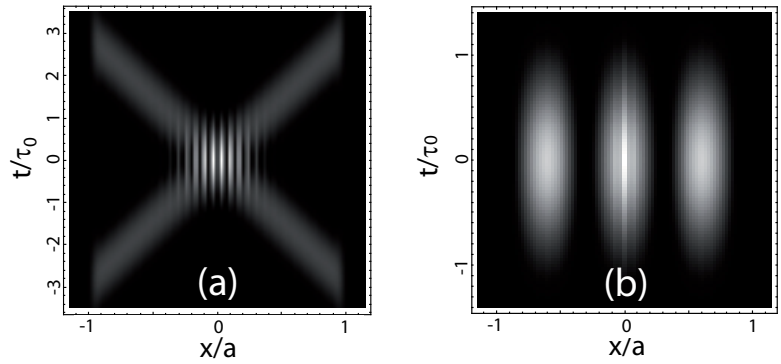

Fig. 6. Temporal evolution of the intensity as a interference of two spatial top-hat ultrafast beams with (a) $a = 1.4$ mm and (b) $a = 70\,\mu$m, for the case $s = f$ and $b = \pm 1.4$ mm. The axial extents are shown in relation to the radius a. The parameters are the same than in Fig. 2.

When the top-hat size is large [see Fig. 6(a)], each pulse arrives independently at the focal plane with opposite incidence angles so that the central position, $x = 0$, is simultaneously reached. The parameter b defines the angle of incidence of each individual pulse as well as the interference pattern in the center of the figure. The lapse of time between the pulses varies linearly along x in a well-defined fashion. The greatest lapse of time, shown in Fig. 6(a), is $\Delta t = 5\tau_0$, although it can be easily changed just by varying the value b in the computer generated hologram. According to (22), $\Delta t = 2ba/fc$. In addition, both pulses fully overlap in the focal plane (but in different times) showing exactly the same intensity along x. These features can be useful in high precision spatial pump-probe experiments [32] without using delay lines.

On the other hand, it is possible to obtain an interference fringe pattern of constant intensity using top-hat profiles having small size, as shown in Fig. 6(b). The interference period and the position of the maximum intensity fringes can be controlled by just changing b and the relative phase of the signal at the SLM. Furthermore, signals involving the generation of a large number of pulses can be used to create interference patterns with hard profiles, such as $\frac{1}{2}\left(1+\cos^n\left(2\pi x/\Lambda+\phi\right)\right)$ along x and $\frac{1}{4}\left(1+\cos^n\left(2\pi x/\Lambda_x+\phi_x\right)\right)\left(1+\cos^m\left(2\pi y/\Lambda_y+\phi_y\right)\right)$ in the transverse plane. In these expressions Λ, ϕ, n and m, are the interference period, relative phase, and integers, respectively. Proper choice of n and m can perform subwavelength ablation patterns of constant depth, controlled by the signal in an approach with no moving parts.

5.3. Pulses with nonstationary orbital angular momentum

In this example, a novel class of ultrashort pulses possessing nonstationary OAM is presented. This kind of pulses could be used in laser-matter interaction to determine the role of the OAM in electron relaxation and in the early plasma formation among many interesting phenomena involving this light property. The key to these pulse generation is to encode a signal composed by LG beams having different OAM and different beam waists, in such a way that the intensity distribution of each LG beam at the SLM do not overlap. This condition ensures that the pulselets neither overlap at the focal plane. If $s > f$ the intensity will have a spherical arrival-time,

#194284 - $15.00 USD Received 22 Jul 2013; revised 25 Sep 2013; accepted 25 Sep 2013; published 11 Oct 2013

so that first pulselet arriving to the focus will be that possessing the higher waist and, thus, in latter times, those having smaller waists. The OAM evolves in time from the outside to the center achieving a global nonstationary orbital angular momentum.

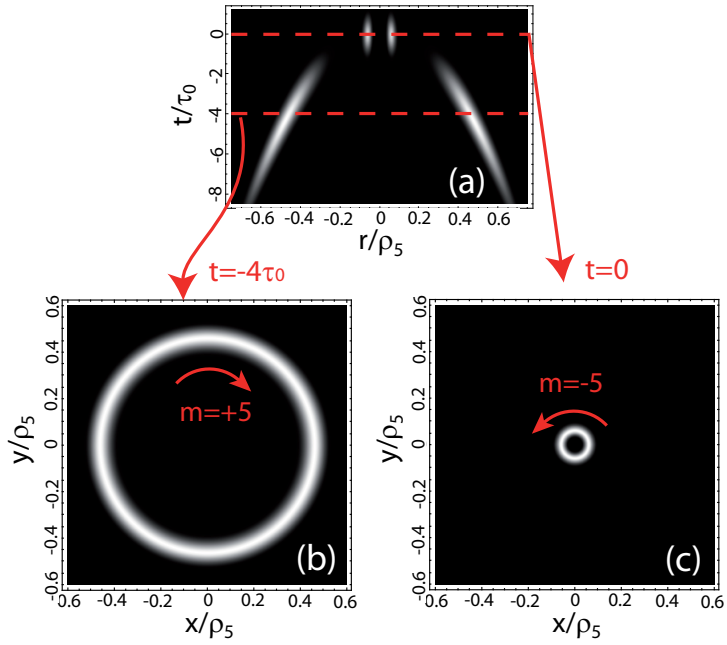

Fig. 7. (a) Temporal evolution of the intensity at the focal plane by using a signal composed by the superposition of $LG_{0,5}$ and $LG_{0,-5}$ modes with $w_0 = 50$ and $400\,\mu$m, respectively. Transverse intensity evaluated at the snapshots $t = -4\tau_0$ (b) and $t = 0$ (c). The topological charge jumps from $m = 5$ to $m = -5$ as the pulse evolves in time.

Figure 7 shows this effect for a signal composed by the superposition of $LG_{0,5}$ and $LG_{0,-5}$ modes with $w_0 = 50$ and $400\,\mu$m, respectively, in the approach $s = 5f$. The ultrashort pulse is composed by two pulselets arriving at the focal plane in different times [see Fig. 7(a)]. A detailed analysis of the transverse intensity is displayed in Figs. 7(b)-7(c) for the snapshots $t = -4\tau_0$ and $t = 0$, respectively. As it can be seen, the topological charge drastically jumps from $m = 5$ to $m = -5$ as the pulse evolves in time.

6. Discussion and conclusion

The usefulness of using SLMs to spatial pulse shaping at the focal plane of a convergence lens (spherical mirror) was presented. To this, the spatial and temporal dependence of the shaped pulse was found by a physically intuitive and efficient procedure. The signal, encoded in the computer generated hologram, was expanded in an orthonormal basis composed of Laguerre-Gaussian modes, in such a way that the pulse at the focus is just the weighted sum of the propagated LG pulselets. Thus, the signal and the pulse are strongly related by the expansion coefficients. Closed-form expressions for the LG pulselets were derived taking advantage of a considerable simplification of the numerical-computational effort. Equation (16) for the Gaussian pulse $(n = 0, m = 0)$ and evaluated for $\omega_0 = 0$ agrees with the well known result [33]. The pulselets are space-time localized wave packets propagating in free space, different from the isodifractive ultrashort Laguerre-Gaussian beams previously found [34]. The frequency components of the pulse in [34] have the same Rayleigh range, that is not the case for (16). The

#194284 - $15.00 USD Received 22 Jul 2013; revised 25 Sep 2013; accepted 25 Sep 2013; published 11 Oct 2013

pulselets behavior determines the properties of the shaped pulse allowing for a physically intuitive description.

In practice, the expansion was truncated by a finite number of terms whose error can be easily monitored and controlled by a well-defined error function. It has been demonstrated that a proper truncation reproduces the signal at the SLM and the wavefield at the focus robustly.

The expansion method was also applied to solve the inverse problem, allowing us to find the proper signal for spatial pulse shaping without using algorithms to solve the phase retrieval problem. The expansion method calculates the electric field of the ultrashort pulse at the focus, even for very short pulses with broad spectral bandwidth. This advance permits to design complex ultrashort wavefield structures in a very simple manner, such as the ones suggested in Section 5. Spatial top-hat and annular ultrafast beam profiles were easily generated. The interference of top-hat pulses by just duplicating and displacing the signal at the SLM along a transverse axis was also illustrated showing as a cumbersome problem can be properly tackled by this method. Top-hat pulses having large spatial size arrives at focal plane independently and within a lapse of time between pulses varying linearly along x. On the one hand, these results could be applied in high precision pump-probe experiments without delay lines. On the other hand, the interference of small size top-hat pulses could create subwavelength ablation patterns in an approach with no moving parts.

The analysis of the pulselets, in addition to issues related to the LG expansion, is relevant since pulses with OAM are implemented recently to optical trapping [35] and to micro and nano machining [36], leading to unique material responses such as ring shaped structures and formation of nanocavities [37]. Further research is necessary to determine if the OAM of the optical vortex pulse could create clearer and smoother processed surfaces and produce chiral microneedle, as demonstrated in the nanoscale time regime [38, 39]. Femtosecond laser vortex pulses have also been applied to fundamental studies in laser-matter interaction such as nonlinear effects and filamentation [40–44] and in characterizing topological properties of materials [12]. In most experimental applications the spatial and temporal evolution of the pulses at the focal plane have not been considered. The assumption of constant pulse arrival time and duration only works well if the mode effective radius is small enough, no matter the distance between the SLM and the lens. When this condition is not met, it is possible to design pulselets in which the arrival time evolves from the outside towards the center (or vice versa), by just setting the distance between the SLM and the lens to satisfy $s > f$ ($s < f$). Moreover, a proper combination of pulselets can create a pulse having a nonstationary orbital angular momentum. These exotic pulses may also be applied to analyze physical phenomena whose characteristic response-time would be of the order of the pulse duration, such as the electron relaxation and the early plasma formation, and also, to determine the role of the optical vortex pulse in the ablation signature. Besides, it would be feasible to control conditions of photoionization in obtaining new selection rules for application in Laser Induced Breakdown Spectroscopy, as demonstrated for monochromatic light [45, 46].

Acknowledgments

We thank José A. Rodrigo and Tatiana Alieva for valuable advice and Paqui, Óscar and Juana for invaluable support. The financial support from the Spanish *Ministerio de Economía y Competividad* under projects TEC 2011-23629, CTQ2008-02578/BQU, CTQ2012-37404-C02-01 and Consolider SAUUL CSD2007-00013 and from *Conselho Nacional de Desenvolvimento Científico e Tecnológico* (CNPq), Brazil, under project 477260/2010-1, are acknowledged. P.V. acknowledges a PQ fellowship of CNPq. The publication of this work was supported by *Servicio Nacional de Aprendizagem Industrial* (SENAI) - DR/Bahia, Brazil.